

Hydrogen density in nanostructured carbon, metals and complex materials

Andreas Züttel^{a,*}, Pascal Wenger^a, Patrick Sudan^a, Philippe Mauron^a, Shin-ichi Orimo^b

^a Physics Department, University of Fribourg, Pérolles, CH-1700 Fribourg, Switzerland

^b Institute for Materials Research, Tohoku University, Sendai 980-8577, Japan

The challenge in the research on hydrogen storage materials is to pack hydrogen atoms or molecules as close as possible. Hydrogen absorbed in metals can reach a density of more than 150 kg m^{-3} (e.g. Mg_2FeH_6 or $\text{Al}(\text{BH}_4)_3$) at atmospheric pressure. For metallic hydrides, however, due to the large atomic mass of the transition metals the gravimetric hydrogen density is limited to less than 5 mass%. Nanostructured carbon materials, e.g. carbon nanotubes or high surface area graphite absorb hydrogen at liquid nitrogen proportional to the specific surface area $1.5 \text{ mass\%/1000 m}^2 \text{ g}^{-1}$. Light weight group three metals, e.g. Al, B, are able to bind four hydrogen atoms and form together with an alkali metal an ionic or at least partially covalent compound. The complex hydrides can only be cycled in as nanostructured materials.

Keywords: Hydrogen; Nanostructures; Volumetric density; Metal hydride; Complexes

1. Introduction

In the hydrogen molecule, the binding σ -orbital in the ground state is filled with two electrons and the antibinding σ^* -orbital is empty. Therefore, the interaction of hydrogen with the surface of a solid can be of two types only physisorption of hydrogen molecules or chemisorption of hydrogen atoms. The reaction of hydrogen gas with a host metal is called the absorption process and can be described in terms of a simplified one-dimensional potential energy curve (one-dimensional Lennard–Jones potential) [1]. Far from the metal surface the potential of a hydrogen molecule and of two hydrogen atoms are separated by the dissociation energy ($\text{H}_2 \rightarrow 2\text{H}$, $E_D = 435.99 \text{ kJ mol}^{-1}$). The attractive interaction of the hydrogen molecule approaching the metal surface is the Van der Waals force leading to the physisorbed state ($E_{\text{Phys}} \approx 10 \text{ kJ mol}^{-1} \text{ H}_2$) approximately one hydrogen molecule radius ($\approx 0.2 \text{ nm}$) from the metal surface. The adsorption of a gas on a surface is a consequence of the field force at the surface of the solid, called the adsorbent, which attracts the molecules of the gas or vapor. The origin of the physisorption of gas molecules on the surface of a solid are resonant fluctuations of the charge distributions and are therefore called dispersive interactions

or Van der Waals interactions. In the physisorption process a gas molecule interacts with several atoms at the surface of the solid. The interaction is composed of two terms: an attractive term which diminishes with the distance between the molecule and the surface to the power of -6 and a repulsive term (Pauli-repulsion) which diminishes with the distance to the power of -12 . H_2 acts as neutral but polarizable adsorbate. Therefore, the potential energy of the molecule shows a minimum at a distance of approximately one molecular radius of the adsorbate. The energy minimum is of the order of 0.01 to 0.1 eV (1 to 10 kJ mol^{-1}) [2]. Due to the weak interaction, a significant physisorption is only observed at low temperatures ($< 273 \text{ K}$). Once a monolayer of adsorbate molecules is formed the gaseous molecule interact with a surface of the liquid adsorbate. Therefore, the binding energy of the second layer of adsorbate molecules is similar to the latent heat of sublimation or vaporization of the adsorbate. Consequently, the adsorption of the adsorbate at a temperature greater to the boiling point at a given pressure leads to the adsorption of one single monolayer [3]. In order to estimate the quantity of adsorbate in the monolayer the density of the liquid adsorbate and the volume of the molecule must be used. If the liquid is assumed to consist of a closed packed fcc structure, the minimum surface area S_{ml} for one mol of adsorbate in a monolayer on a substrate can be calculated from the density of the liquid ρ_{liq} and the molecular mass of the adsorbate M_{ads} .

* Corresponding author. Tel.: +41-26-300-9086;
fax: +41-26-300-9747.
E-mail address: andreas.zuettel@unifr.ch (A. Züttel).

$$S_{\text{ml}} = \frac{\sqrt{3}}{2} \left(\sqrt{2N_A} \frac{M_{\text{ads}}}{\rho_{\text{liq}}} \right)^{2/3} \quad (1)$$

N_A stands for the Avogadro constant ($N_A = 6.022 \times 10^{23} \text{ mol}^{-1}$). The monolayer surface area for hydrogen is $S_{\text{ml}}(\text{H}_2) = 85917 \text{ m}^2 \text{ mol}^{-1}$. The amount of adsorbate m_{ads} on a substrate material with a specific surface area S_{spec} is then given by $m_{\text{ads}} = M_{\text{ads}} S_{\text{spec}} / S_{\text{ml}}$. Therefore, the density of physisorbed hydrogen is limited to the density of liquid hydrogen ($\rho_{\text{liq.}} = 70.8 \text{ kg m}^{-3}$).

Closer to the surface of simple and noble metals the antibonding $1\sigma^*$ level of H_2 overlaps with the metal (M) levels of the same symmetry and increases the energy of the H_2 molecules, i.e. weaken the H–H bonding state. If the energy of H_2 -molecule is sufficient to overcome the activation barrier for dissociation the H–H bond breaks up and the hydrogen-metal bond is formed. The height of the activation barrier depends on the surface elements involved. Hydrogen atoms sharing their electron with the metal atoms at the surface are then in the chemisorbed state ($E_{\text{Chem}} \approx 50 \text{ kJ mol}^{-1} \text{ H}_2$). The chemisorbed hydrogen atoms may have a high surface mobility, interact with each other and form surface phases at sufficiently high coverage. In the next step the chemisorbed hydrogen atom can jump in the subsurface layer, and finally diffuse on the interstitial sites through the host metal lattice. The hydrogen atoms contribute with their electron to the band structure of the metal. The hydrogen is at small hydrogen to metal ratio ($H/M < 0.1$) exothermically dissolved (solid-solution, α -phase) in the metal. The metal lattice expands proportional to the hydrogen concentration by approximately $2\text{--}3 \text{ \AA}^3$ per hydrogen atom [4]. At greater hydrogen concentrations in the host metal ($H/M > 0.1$) a strong H–H interaction due to the lattice expansion becomes important and the hydride phase (β -phase) nucleates and grows. The hydrogen concentration in the hydride phase is often found to be $H/M = 1$. The volume expansion between the coexisting α - and the β -phase corresponds in many cases 10–20% of the metal lattice. Therefore, at the phase boundary large stress is built up and often leads to a decrepitation of brittle host metals such as intermetallic compounds. The final hydride is a powder with a typical particle size of 10–100 μm . The thermodynamic aspects of the hydride formation from gaseous hydrogen is described by means of pressure-composition isotherms (Fig. 4). While the solid solution and hydride phase coexists, the isotherms show a flat plateau, the length of which determines the amount of H_2 stored. In the pure β -phase, the H_2 pressure rises steeply with the concentration. The two-phase region ends in a critical point T_C , above which the transition from α - to β -phase is continuous. The equilibrium pressure p_{eq} as a function of temperature is related to the changes ΔH and ΔS of enthalpy and entropy, respectively, by the Van't Hoff equation:

$$\ln \left(\frac{p_{\text{eq}}}{p_{\text{eq}}^0} \right) = \frac{\Delta H}{R} \frac{1}{T} - \frac{\Delta S}{R} \quad (2)$$

As the entropy change corresponds mostly to the change from molecular hydrogen gas to dissolved solid hydrogen, it amounts approximately to the standard entropy of hydrogen ($S^0 = 130 \text{ J K}^{-1} \text{ mol}^{-1}$) and is therefore, $\Delta S_f \approx -130 \text{ J K}^{-1} \text{ mol}^{-1} \text{ H}_2$ for all metal–hydrogen systems. The enthalpy term characterizes the stability of the metal hydrogen bond.

Several empirical models allow the estimation of the stability and the amount of hydrogen in an intermetallic hydride. The maximum amount of hydrogen in the hydride phase is given by the number of interstitial sites in the intermetallic compound for which the following two criteria do apply. The distance between two hydrogen atoms on interstitial sites is at least 2.1 \AA [5] and the radius of the largest sphere on an interstitial site touching all the neighboring metallic atoms is at least 0.37 \AA (Westlake criterion) [6]. The theoretical maximum volumetric density of hydrogen in a metal hydride, assuming a closed packing of the hydrogen, is therefore 253 kg m^{-3} , which is 3.6 times the density of liquid hydrogen. The maximum density found in hydrides reaches 150 kg m^{-3} for Mg_2FeH_6 and $\text{Al}(\text{BH}_4)_3$ [7]. All hydrides known with a gravimetric hydrogen density greater than 3 mass% undergo a metal-semiconductor or a metal insulator transition upon hydrogen absorption. Typical diffusion coefficients in bcc metallic hydrides are of the order of $10^{-6} \text{ cm}^2 \text{ s}^{-1}$ and in fcc metallic hydrides of the order of $10^{-9} \text{ cm}^2 \text{ s}^{-1}$.

The physical properties of materials are size dependent, significant changes can be observed when the particles or agglomerates are smaller than 10 nm. The specific surface area increases with decreasing characteristic length, e.g. diameter of the particles as shown in Fig. 1. Therefore also the ratio of surface atoms to bulk atoms increases when the diameter of the particles is reduced. The most obvious change is the crystal structure or better the geometrical arrangement of the atoms when the size of agglomerates of atoms is in the nanometer range. The crystal structure of bulky materials in thermal equilibrium is defined by the minimum of the Gibbs free enthalpy (ΔG). However, agglomerates of a few hundred atoms are dominated by the surface energy and usually form regular polyhedrons, e.g. icosaheder, cuboctaheder or Wulff-polyheder (Fig. 2). Such particles are usually called clusters. These polyhedrons tend to agglomerate in order to reduce the surface area and therefore the energy and crystallize to bulk material. The melting temperature of gold particles decreases with decreasing size [8] clearly indicating the increased energy and lower stability of gold clusters as compared to bulk gold particles. The electronic structure in a confined cluster is different from the electronic structure in an infinite bulk lattice. This has been shown for palladium clusters [9] where the d-band exhibits a reduced band with as the size of the cluster is decreased. Furthermore, significant changes at the Fermi energy E_F and for the unoccupied states above E_F are observed.

The increased specific surface area together with the short diffusion paths and the lower stability of clusters as

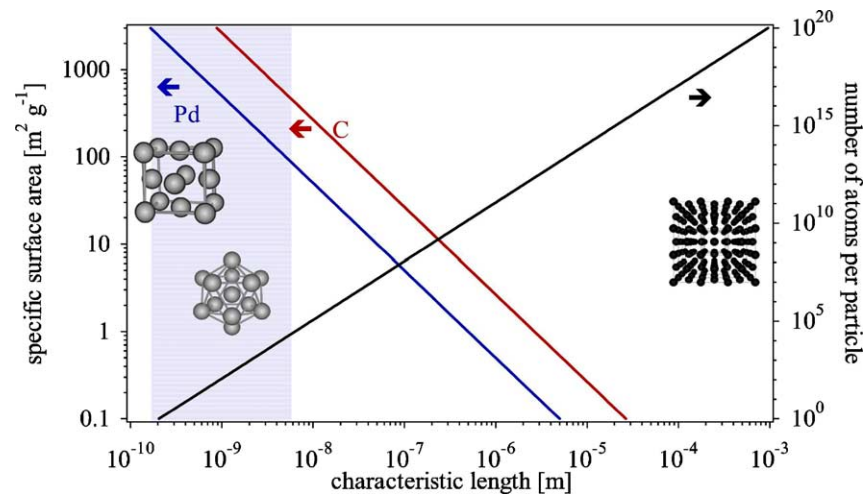


Fig. 1. Specific surface area (left axis) and number of atoms per particle (right axis) as a function of the characteristic length such as the diameter of the particle. The insets show a bulk lattice (3×10^{-4} m), a cluster (2×10^{-9} m), and a unit cell (2×10^{-10} m).

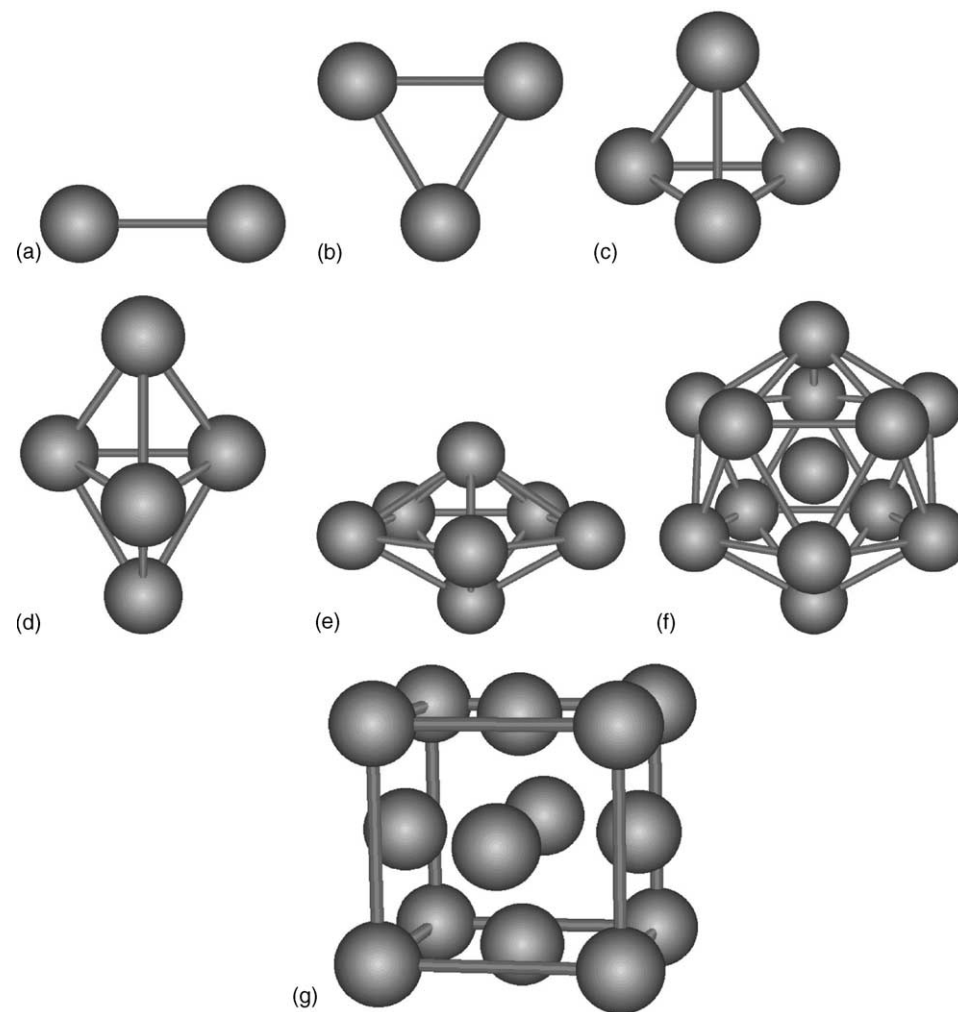


Fig. 2. The growth mechanism of clusters of ideal spherical atoms was calculated by Northby [54]. Starting with two single atoms a dimer, $N = 2$ is formed. The trimer, $N = 3$, has the geometry of an equilateral triangle; $N = 4$ corresponds to a tetrahedron, $N = 5$ to a triangular bipyramid. For $N = 7$ the cluster appears as a pentagonal bipyramid, i.e. a ring of five atoms, with one atom above and one below it. The smallest member of the clusters with icosahedral geometry is observed for $N = 13$, one interior atom with two pentagonal caps, i.e. an icosahedron.

compared to bulk material make them interesting for the investigation of the interaction with hydrogen. Furthermore, hydride which only form as surface layers in bulk state due to passivation, e.g. MgH_2 can be investigated as cluster samples. New hydrogen sorption properties may be expected for metallic clusters because of different types of interstitial sites and modified electronic band structures as compared to the bulk. The investigation of size dependant properties leads to a deeper insight in the local properties of hydrides.

2. Hydrogen in metallic-clusters

Palladium is a noble metal and has a reasonably high hydrogen storage capacity (0.6H/Pd). Metal clusters evaporated on a substrate usually show a wide size distribution. Properties determined from such a cluster sample are always averaged over a large range in cluster size. Thermodynamic properties of the Pd-H system were studied on 3.1 and 3.6 nm clusters in the gas phase by Pundt et al. [10]. To avoid interfacial stress that occurs between an adhering particle and the substrate, the clusters were embedded in an elastic soft polymer matrix and in a surfactant shell, respectively. A largely enhanced H-solubility was found in the α -phase region. Additionally the solubility limit of the α -phase is shifted to a higher H-concentration whereas the minimum β -phase solubility is lowered compared to that of bulk Pd. This can be attributed to an occupation of subsurface sites. Sorption-desorption isotherms show the existence of a small hysteresis. This hysteresis can not be related to the formation of misfit dislocations because of the small cluster size, but can be explained with regard to the thermodynamics of an open two-phase system with coherent interfaces.

In order to investigate size-dependent properties of the clusters either single isolated clusters or cluster samples with a very narrow size distribution were examined [11]. Large clusters samples (≈ 1 g) of some noble elements, e.g. Pd, with a narrow size distribution were synthesized by the reduction of the metal ions with hydrogen gas in a solution of Pd^{II} -acetate. The metal atoms form a cluster and organic ligands bind to the surface of the cluster. The ligand shell (e.g. phenantroline) stabilizes the clusters and prevents cluster agglomeration. By simple drying in air stable black cluster-powder is achieved [11].

The structural and hydriding properties of three monodispersed cluster samples $\text{Pd}^{7/8}$ (95% of 7 shell clusters and 5% of 8 shell clusters), Pd^5 (5 shell clusters), Pd^2 (2 shell clusters) and Pd bulk powder (particle size $\approx 50 \mu\text{m}$) have been investigated [12].

The icosahedron can be constructed from 20 slightly distorted fcc unit cells, whose faces are (1 1 1) planes and which share common vertex. The inter atomic spacing is not uniform in an icosahedron. This leads to a built-up mechanical stresses, so that for large N ($N = 1500$) the fcc lattice becomes favored.

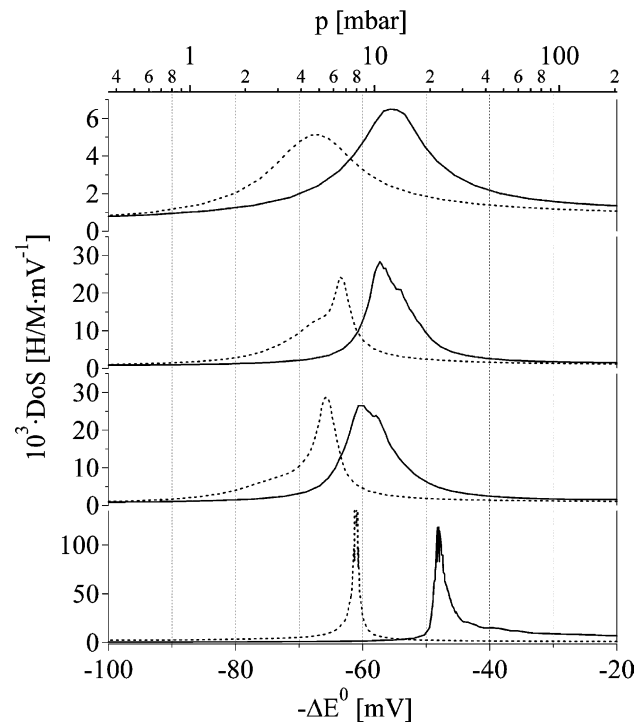


Fig. 3. Density of states (DoS) for hydrogen calculated from the concentration vs. the equilibrium potential curve for bulk Pd, $\text{Pd}^{7/8}$ cluster, Pd^5 cluster, and Pd^2 (from bottom to top). Solid lines represent the absorption and broken lines the desorption.

The three cluster samples $\text{Pd}^{7/8}$, Pd^5 and Pd^2 exhibit diffraction peaks at the same position as bulk Pd and therefore the lattice parameters calculated from the refinement of the diffraction pattern are the same for the cluster samples and bulk Pd within the accuracy of the calculation. The small size¹ as well as the mechanical stress in the cluster leads to peak broadening. There are indications that the outer most shell of an icosahedral cluster is closer to the second most outer shell than all the other inter-shell distances [13,14]. Fig. 3 shows the density of states for hydrogen (DoS) as a function of the equilibrium potential (ΔE^0), i.e. the first derivative of the hydrogen concentration over the equilibrium potential. Bulk Pd exhibits a narrow DoS distribution. With decreasing size of the clusters the width of the DoS distribution increases. Furthermore, the distance between the maximum in the DoS distribution for absorption and desorption increases with decreasing cluster size. In the size range from 7/8 shells to 2 shells the hydrogen sorption properties are strongly size dependent. The pronounced phase transition from Pd to $\text{PdH}_{0.6}$ which is found for bulk Pd is still observed in the cluster samples, however in a less clear form. The increasing width of the DoS distribution is also observed for bulk Pd at elevated temperatures, i.e. close to

¹ Geometrically the diameter of the icosahedron surrounding sphere, i.e. the Pd cluster diameter is calculated according to the equation $d = n \cdots a_{\text{fcc}} \cdots 0.5 \cdots \sqrt{5 + \sqrt{5}}$ where a_{fcc} stands for the lattice parameter of fcc palladium and n for the number of shells.

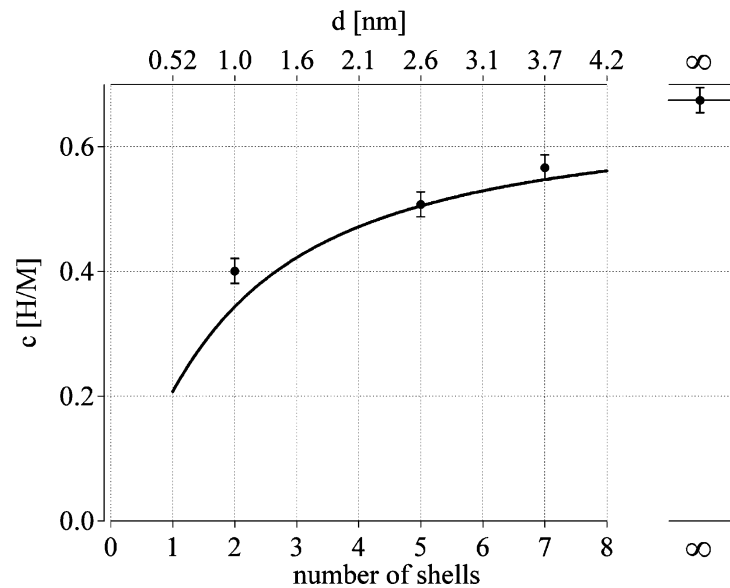


Fig. 4. Hydrogen capacity as a function of the number of shells in the Pd clusters. The line represents the calculated capacity according to the model (Eq. (3)) and the markers stand for the measured capacities. Bulk Pd is placed at an infinite number of shells. Hundred percent of capacity corresponds to $\text{PdH}_{0.67}$.

the critical temperature (T_c (bulk Pd) = 571 K [15]). The critical temperature for the hydride formation of the clusters is probably size dependent and decreases with decreasing cluster size. The capacity decreases with decreasing cluster size. Hydrogen usually occupies tetrahedral or octahedral interstitial sites in the host metal. A fcc structure offers 1 octahedral and two tetrahedral interstitial sites per metal atom for hydrogen. By the simple assumption that surface atoms provide less interstitial sites for hydrogen, the capacities for different cluster sizes were calculated: at corners 0.25 H/M (H atoms per metal atom), at edges 0.4 H/M and at faces 0.5 H/M.

$$C[\text{H}] = 0.6 \left\{ 4 + (n - 1) \left(4 + \frac{10}{3} n(n + 1) \right) \right\} \quad (3)$$

where n is the number of shells in the Pd-cluster and $C[\text{H}]$ the capacity in hydrogen-atoms for the hole cluster with n shells (Fig. 4).

The calculated capacities according to the model above agree very well with the measured capacities for Pd bulk powder (particle size $\approx 50 \mu\text{m}$), $\text{Pd}^{7/8}$ clusters, Pd^5 cluster and Pd^2 clusters.

3. Hydrogen in carbon nanotubes

Much work on reversible hydrogen sorption of carbon nanostructures was stimulated by findings published in an article from Dillon et al. [16]. This paper describes the results of a brief hydrogen desorption experiment. The authors estimated the hydrogen storage capacity of carbon nanotubes at that time to be 5–10 mass%. The investigation was carried out on a carbon sample containing an estimated (TEM micrographs) amount of 0.1–0.2 mass% of single wall

carbon nanotubes. The amount of hydrogen desorbed in the high-temperature peak, which is roughly 5–10 times smaller than the low temperature physisorption peak, was 0.01 mass%. The authors concluded “Thus, the gravimetric storage density per SWNT ranges from 5 to 10 mass%”. Three years later in a report to the DOE [17] this peak has moved significantly by 300 K up to 600 K. Apparently the reported results are inconsistent. Hirscher et al. [18] clarified the situation and showed that the desorption of hydrogen originates from Ti-alloy particles in the sample, introduced during the ultrasonic treatment, rather than from the carbon nanotubes.

The main difference between carbon nanotubes and high surface area graphite is the curvature of the graphene sheets and the cavity inside the tube. In microporous solids with capillaries which have a width not exceeding a few molecular diameters, the potential fields from opposite walls will overlap so that the attractive force which act up on adsorbate molecules will be increased as compared with that on a flat carbon surface [19]. This phenomenon is the main motivation for the investigation of the hydrogen interaction with carbon nanotubes.

Most papers reporting theoretical studies on hydrogen absorption in carbon nanostructures focus on the physisorption of H_2 on carbon using the grand canonical Monte Carlo simulation. Stan and Cole [20] used the Feynman (semiclassical) effective potential approximation to calculate the adsorption potential and the amount of hydrogen adsorbed on a zigzag nanotube (13,0) with a diameter of 1.018 nm. The adsorption potential was found to be 9 kJ mol^{-1} (0.093 eV) for hydrogen molecules inside the nanotubes at 50 K, the potential is about 25% higher as compared to the flat surface of graphite due to the curvature of the surface. Therefore,

an increased number of carbon atoms interacts with the hydrogen molecule. The ratio of hydrogen adsorbed in the tube to that on a flat surface decreases strongly with increasing temperature and is 10,000 at 50 K and 100 at 77 K (values taken from figure). Rzepka et al. [21] used a grand canonical ensemble Monte Carlo program to calculate the amount of adsorbed hydrogen for a slit pore and a tubular geometry. The amount of adsorbed hydrogen depends on the surface area of the sample, the maximum is at 0.6 mass% ($P = 6$ MPa, $T = 300$ K). The calculation was experimentally verified with excellent agreement. At a temperature of 77 K the amount of adsorbed hydrogen is about one order of magnitude higher compared to 300 K. Williams and Eklund [22] performed grand canonical Monte Carlo simulation of H_2 physisorption in finite-diameter carbon SWNT ropes and found an increasing amount of adsorbed hydrogen with decreasing temperature from 1.4 mass% ($P = 10$ MPa, $T = 300$ K) to 9.6 mass% ($P = 10$ MPa, $T = 77$ K). For lower hydrogen pressure this range is shifted to considerably lower amounts of adsorbed hydrogen, i.e. 0.2 mass% ($P = 1$ MPa, $T = 300$ K) to 5.9 mass% ($P = 10$ MPa, $T = 77$ K). Lee et al. [23] have performed density-functional and density-functional-based tight binding calculations to search for hydrogen chemisorption sites on single wall-nanotubes. The investigation of the absorption of the hydrogen inside the tubes has shown that it is energetically more favorable for the hydrogen atoms to recombine and form molecules, which are then physisorbed inside the nanotube. Ma et al. [24] performed a molecular dynamics simulation for H implantation. The hydrogen atoms (20 eV) were implanted through the side walls of a single wall carbon nanotube (5,5) consisting of 150 atoms and have a diameter of 0.683 nm.

They found that the hydrogen atoms recombine to molecules inside the tube and arrange themselves to a concentric tube. The hydrogen pressure inside the SWNT increases as the number of injected atoms increases and reaches 35 GPa for 90 atoms (5 mass%). This simulation does not exhibit a condensation of hydrogen inside the nanotube. The critical temperature of hydrogen (H_2) is 33.25 K [25]. Therefore, at temperatures above 33.25 K and at all pressures hydrogen does not exist as a liquid phase, hydrogen is either a gas or a solid. The density of liquid and solid hydrogen at the melting point ($T_m = 14.1$ K) is 70.8 and 70.6 kg m $^{-3}$, respectively. The measurement of the latent heat of condensation of nitrogen on carbon black [26] showed, that the heat for the adsorption of one monolayer is between 11 and 12 kJ mol $^{-1}$ (0.11–0.12 eV) and drops for subsequent layers to the latent heat of condensation for nitrogen which is 5.56 kJ mol $^{-1}$ (0.058 eV). If we assume, that hydrogen behaves similar to nitrogen, hydrogen would only form one monolayer of liquid at the surface of carbon at temperatures above the boiling point. Geometrical considerations of the nanotubes lead to the specific surface area and therefore, to the maximum amount of condensed hydrogen in a surface monolayer. Fig. 5 shows the maximum amount of hydrogen in mass% for the physisorption of hydrogen on carbon nanotubes [27]. The maximum amount of adsorbed hydrogen is 2.0 mass% for single wall carbon nanotubes (SWNT) with a specific surface area of 1315 m 2 g $^{-1}$ at a temperature of 77 K.

Experiments on hydrogen absorption in carbon nanostructures were carried out with different methods under various conditions and on plenty of small and often not very well characterized samples. Hydrogen gas adsorption isotherms ($T = 80$ K) were performed by Ye et al. on

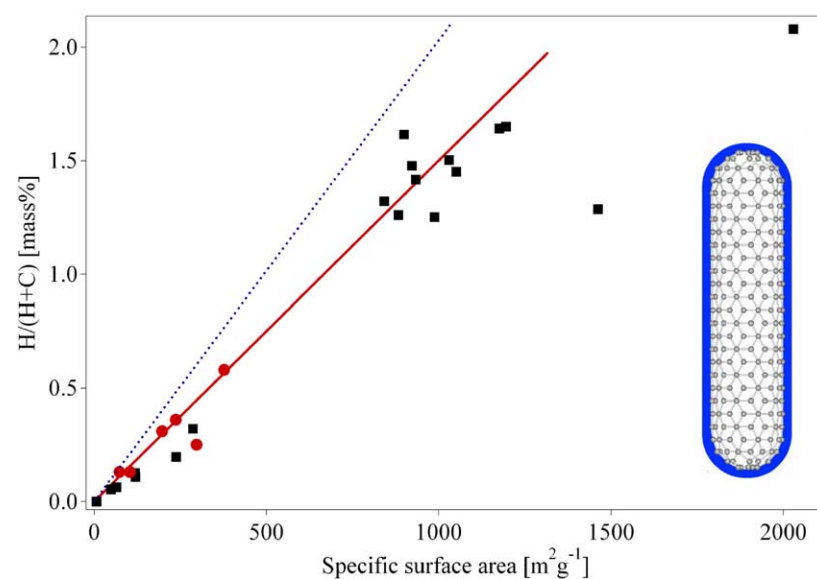


Fig. 5. Reversible amount of hydrogen (electrochemical measurement at 298 K) vs. the B.E.T. surface area (round markers) of a few carbon nanotube samples including two measurements on high surface area graphite (HSAG) samples together with the fitted line. Hydrogen gas adsorption measurements at 77 K from Nijkamp et al. [35] (square markers) are included. The dotted line represents the calculated amount of hydrogen in a monolayer at the surface of the substrate.

purified SWNT samples [28]. The BET surface area of the SWNT sample was found to be $285\text{ m}^2\text{ g}^{-1}$ and remained unchanged upon the hydrogen absorption and desorption. The hydrogen adsorption obtained at a temperature of 80 K and a pressure of 0.32 MPa was $H/C = 0.04$ for the SWNT sample and was $H/C = 0.28$ for the high surface area saran-carbon ($1600\text{ m}^2\text{ g}^{-1}$). At high hydrogen pressures (7 MPa) at a temperature of 80 K the hydrogen to carbon ratio for the SWNT sample reached $H/C = 1$ (7.7 mass%) in the initial absorption. In the following absorption cycles the absorption isotherm considerably shifted to higher pressure. The hydrogen to carbon ratio of $H/C = 0.8$ was reached at 12 MPa. Liu et al. [29] applied high pressure (12 MPa) hydrogen gas at room temperature (298 K) to SWNT and followed the pressure change in time. The samples equilibrated after approximately 300 min and reached a maximum absorption of 4.2 mass% ($H/C = 0.5$). About 20% of the absorbed hydrogen remained in the sample after desorption at room temperature. Fan et al. [30] investigated the hydrogen absorption of vapor-grown carbon nanofibers with a diameter of 5–300 nm. The fibers absorbed hydrogen up to 12.38 mass% when a hydrogen pressure of 12 MPa was applied. The absorption equilibrated upon 200–300 min. Chen et al. [31] reported that a high hydrogen uptake of 14 mass% to 20 mass% can be achieved for K- and Li-doped MWNT, respectively, at a pressure of 0.1 MPa. The K-doped MWNT absorb hydrogen at room temperature, but they are chemically unstable, whereas the Li-doped MWNT are chemically stable, but require elevated temperatures (473–673 K) for maximum absorption and desorption of hydrogen. However, the increase of the mass observed upon hydrogen absorption was due to impurities like oxygen and water and therefore due to the oxidation of the alkali metals [32] rather than a hydrogen uptake. A large variety of carbon samples was investigated by Ströbel et al. [33], using a high-pressure microbalance. The BET (N_2) surface area of the samples ranges from $100\text{ m}^2\text{ g}^{-1}$ up to $3300\text{ m}^2\text{ g}^{-1}$. The absorbed amount of hydrogen ($P = 12.5\text{ MPa}$, $T = 296\text{ K}$) correlates with the surface area according to the equation $\times [\text{mass}\%] = 0.0005S (\text{m}^2\text{ g}^{-1})$ (taken from figure) except for the nano fiber samples. The latter exhibit a rather low surface area of approximately $100\text{ m}^2\text{ g}^{-1}$; however, the increase in mass upon hydrogen absorption corresponds to about 1.2 mass%. The measured adsorption isotherms approximately follow the Langmuir adsorption model. Some isotherms intercept the mass-axis ($P = 0$) at $x = 0$, other intercept at a finite mass between 0.2 and 0.4 mass%. Nijkamp et al. [34] characterised a large number of carbonaceous sorbents using N_2 physisorption at 77 K and up to a pressure of 1 bar. The sorbents were chosen to represent a large variation in surface areas and (micropores) volumes. Both non-porous materials, such as aerosil and graphites, and microporous sorbents, such as activated carbons and zeolites, were selected. The H_2 -adsorption measurements were performed at 77 K in the pressure range 0–1 bar. From adsorption–desorption experiments it is evident that reversible physisorption takes

place exclusively with all samples. The amount of adsorbed hydrogen correlates with the specific surface area of the sample (Fig. 5). A few papers on electrochemical measurements at room temperature of hydrogen uptake and release have been published [35–38]. The electrochemical hydrogen absorption is reversible. The maximum discharge capacity measured at 298 K is 2 mass% with a very small discharge current (discharge process for 1000 h). The few round markers with the fitted line in Fig. 5 are electrochemical results. It is remarkable, that the measurements of the hydrogen uptake in the gas phase at 77 K exhibit the same quantities as the electrochemical measurements at room temperature 298 K. In the electrochemical charging process hydrogen atoms are left back at the surface of the electrode when the electron transfer from the conductor to the water molecules takes place. The hydrogen atoms recombine to hydrogen molecules. This process goes on until the surface is completely covered with a monolayer of physisorbed H_2 molecules. Additional hydrogen does not interact with the attractive Van der Waals forces of the surface. The hydrogen molecules become very mobile and form gas bubbles, which are released from the electrode surface. The formation of a stable monolayer of hydrogen at the electrode surface at room temperature is only possible if either the hydrogen atoms or the hydrogen molecules are immobile, i.e. their surface diffusion has to be kinetically hindered by a large energy barrier probably due to the adsorbed electrolyte (H_2O) molecules in the second layer. An other possible reaction path was first reported [23] as a result of density-functional calculation. The result of this calculation is that hydrogen atoms tend to chemisorb at the exterior surface of a nanotube. The atoms can then flip in and recombine to hydrogen molecules finally at high coverage forming a concentric cylinder in the cavity of the nanotube. If the binding energy of the chemisorbed hydrogen is relatively low compared to the energy in hydrocarbons, the absorbed amount of hydrogen is proportional to the surface area of the carbon sample and could also desorb at rather positive electrochemical potential.

In conclusion, the reversible hydrogen sorption process is based on the physisorption. The amount of adsorbed hydrogen is proportional to the BET surface area of the nanostructured carbon sample. The amount of adsorbed hydrogen from the gas phase at 77 K and electrochemically at room temperature is $1.5 \times 10^{-3}\text{ mass}\% \text{ m}^{-2} \text{ g}^{-1}$. Together with the maximum specific surface area of carbon ($1315\text{ m}^2\text{ g}^{-1}$) the maximum absorption capacity of carbon nanostructures is 2 mass%. The experimental results are in good agreement with the theoretical estimations if we take into account that the measurements were carried out at a temperature of 77 K which is still far above the critical temperature of hydrogen of 32 K and therefore the monolayer of hydrogen is not complete at 77 K. No evidence of an influence of the geometric structure of the nanostructured carbon on the amount of absorbed hydrogen was found. It is quite obvious, that the curvature of nanotubes may only influence the adsorption

energy but not the amount of adsorbed hydrogen. Furthermore, all attempts to open the nanotubes and to absorb hydrogen inside the tubes did not show an increased absorption of hydrogen molecules. Theoretical studies beyond the well-known physisorption lead to a large set of various maximum hydrogen absorption capacities. Most of the results were found under special conditions, e.g. at 0 K or high energy hydrogen atom implantation. No evidence was found for a higher density of hydrogen in and on carbon nanostructures compared to liquid hydrogen at ambient conditions.

The big advantages of the physisorption for hydrogen storage are the low operating pressure, the relatively low cost of the materials involved and the simple design of the storage system. The rather small amount of adsorbed hydrogen on carbon together with the low temperatures necessary are significant drawbacks of the hydrogen storage based on physisorption.

4. Hydrogen in zeolites and nanocubes

Beside the carbon nanostructures, other nanoporous materials have been investigated for hydrogen absorption. The hydrogen absorption of zeolites of different pore architecture and composition, e.g. A, X, Y, was analyzed in the temperature range from 293 to 573 K and pressure range from 2.5 to 10 MPa [38]. Hydrogen was absorbed at the desired temperature and pressure. The sample was then cooled to room temperature and evacuated. Subsequently the hydrogen release upon heating of the sample to the absorption temperature was detected. The absorbed amount of hydrogen increased with increasing temperature and increasing absorption pressure. The maximum amount of desorbed hydrogen was found to be 0.08 mass% for a sample loaded at a temperature of 573 K and a pressure of 10 MPa [39]. The adsorption behavior indicates that the absorption is due to a chemical reaction rather than physisorption. At liquid nitrogen temperature (77 K) the zeolites physisorb hydrogen proportional to the specific surface area of the material. A maximum of 1.8 mass% of adsorbed hydrogen was found for a zeolite (NaY) with a specific surface area of $725 \text{ m}^2 \text{ g}^{-1}$ [40]. The low temperature physisorption (type I isotherm) of hydrogen in zeolites is in good agreement with the adsorption model mentioned above for nanostructured carbon. The desorption isotherm followed the same path as the adsorption [40] which indicates that no pore condensation occurred. Recently, a microporous metal-organic framework of the composition $\text{Zn}_4\text{O}(1,4\text{-benzenedicarboxylate})_3$ was proposed as hydrogen storage material [41]. The material absorbs hydrogen at a temperature of 298 K proportional to the applied pressure. The slope of the linear relationship between the gravimetric hydrogen density and the hydrogen pressure was found to be $0.05 \text{ mass\% bar}^{-1}$. No saturation of the hydrogen absorption was found, which is very unlikely for any kind of a hydrogen absorption process. At 77 K the amount of adsorbed hydrogen was detected to be 3.7 mass% already at very low

hydrogen pressure and a slight almost linear increase with increasing pressure. This behavior is not a type I isotherm as the authors claimed and the results should be taken with care.

4.1. Complex hydrides

The group one two and three light metals, e.g. Li, Mg, B, Al, build a large variety of metal-hydrogen complexes. They are especially interesting because of their light weight and the number of hydrogen atoms per metal atom, which is in many cases 2. The main difference of the complex hydrides to the above-described metallic hydrides is the transition to an ionic or covalent compound of the metals upon hydrogen absorption. The hydrogen in the complex hydrides is often located in the corners of a tetrahedron with boron or aluminum in the center. The negative charge of the anion, $[\text{BH}_4]^-$ and $[\text{AlH}_4]^-$ is compensated by a cation e.g. Li or Na. The hydride complexes of borane, the tetrahydroborates $\text{M}(\text{BH}_4)$, and of alane the tetrahydroaluminate $\text{M}(\text{AlH}_4)$ are interesting storage materials, however, they were known to be stable and decompose only at elevated temperatures and often above the melting point of the complex.

Bogdanovič and Swickardi [42] presented in 1996 for the first time adsorption and desorption pressure-concentration isotherms of catalyzed NaAlH_4 at temperature of 180 and 210 °C. The isotherms exhibit an absence of hysteresis and a nearly horizontal pressure plateau. Furthermore, the catalyzed system reversibly absorbed and desorbed hydrogen up to 4.2 mass% and the mechanism of the two step reaction was described. A more detailed study of the NaAlH_4 with an improved catalyst was published in 2000 by Bogdanovič et al. [43]. A desorption hydrogen pressure of 2 bar at 60 °C was found and the enthalpy for the dissociation reaction was determined to be 37 and 47 kJ mol^{-1} for the first dissociation step of Ti-doped NaAlH_4 : $3\text{NaAlH}_4 \rightarrow \text{Na}_3\text{AlH}_6 + 2\text{Al} + 3\text{H}_2$ (3.7 wt.% H) and the second $\text{Na}_3\text{AlH}_6 \rightarrow 3\text{NaH} + \text{Al} + 3/2\text{H}_2$ (3.0 wt.% H), respectively. Therefore, the equilibrium hydrogen pressure at room temperature is approximately 1 bar. Furthermore, the reaction is reversible, a complete conversion to product was achieved at 270 °C under 175 bar hydrogen pressure in 2–3 h [44].

The first report of a pure alkali metal tetrahydroboride appeared in 1940 by Schlesinger and Brown [45] who synthesized the lithiumtetrahydroboride (lithiumborohydride) (LiBH_4) by the reaction of ethyllithium with diborane (B_2H_6). The direct reaction of the corresponding metal with diborane in etheral solvents under suitable conditions produces high yields of the tetrahydroborides [46] $2\text{MH} + \text{B}_2\text{H}_6 \rightarrow 2\text{MBH}_4$ where M: Li, Na, K, etc. Direct synthesis from the metal, boron and hydrogen at 550–700 °C and 30–150 bar H_2 has been reported to yield the lithium salt, and it has been claimed that such a method is generally applicable to groups IA and IIA metals [47]. The reaction involving either the metal or the metal hydride, or the metal together with triethylborane in an inert hydrocarbon has

formed the basis of a patent $M + B + 2H_2 \rightarrow MBH_4$, where M: Li, Na, K, etc.

The stability of metal tetrahydroborides has been discussed in relation to their percentage ionic character, and those compounds with less ionic character than diborane are expected to be highly unstable [48]. Steric effects have also been suggested to be important in some compounds [49,50]. The special feature exhibited by the covalent metal hydroborides is that the hydroboride group is bonded to the metal atom by bridging hydrogen atoms similar to the bonding in diborane, which may be regarded as the simplest of the so called “electron-deficient” molecules. Such molecules possess fewer electrons than those apparently required to fill all the bonding orbital’s, based on the criterion that a normal bonding orbital involving two atoms contains two electrons. The molecular orbital bonding scheme for diborane has been discussed extensively [49].

The compound with the highest gravimetric hydrogen density at room temperature known today is $LiBH_4$ (18 mass%). Therefore, this complex hydride could be the ideal hydrogen storage material for mobile applications. $LiBH_4$ desorbs three of the four hydrogen in the compound upon melting at $280^\circ C$ and decomposes into LiH and boron. The desorption process can be catalyzed by adding SiO_2 and significant thermal desorption was observed starting at

$100^\circ C$ [51]. Recently it has been shown, that the hydrogen desorption reaction is reversible and the end products lithiumhydride and boron absorb hydrogen at $690^\circ C$ and 200 bar to form $LiBH_4$ [52]. The scientific understanding of the mechanism of the thermal hydrogen desorption from $LiBH_4$ and the absorption remains a challenge and more research work has to be carried out. Fichtner et al. [53] have successfully catalyzed $NaAlH_4$ with Ti-clusters consisting of only 13 Ti atoms. The resulting sorption kinetics is superior compared to all other catalytic additives known today. Due to the localisation of the hydrogen in the lattice and the slow diffusion rate of the metals in the solid, hydrogen sorption reactions are only possible in a decent time if the complex materials are nanostructured and the diffusion paths are short.

5. Conclusion

The gravimetric and the volumetric hydrogen density in materials is shown in Fig. 6. The metallic hydrides exhibit a very high volumetric density, exceeding the density of liquid hydrogen by a factor of two. The surface atoms dominate the hydrogen sorption characteristics in nanostructured metals, i.e. the sorption kinetics is increased. However, the

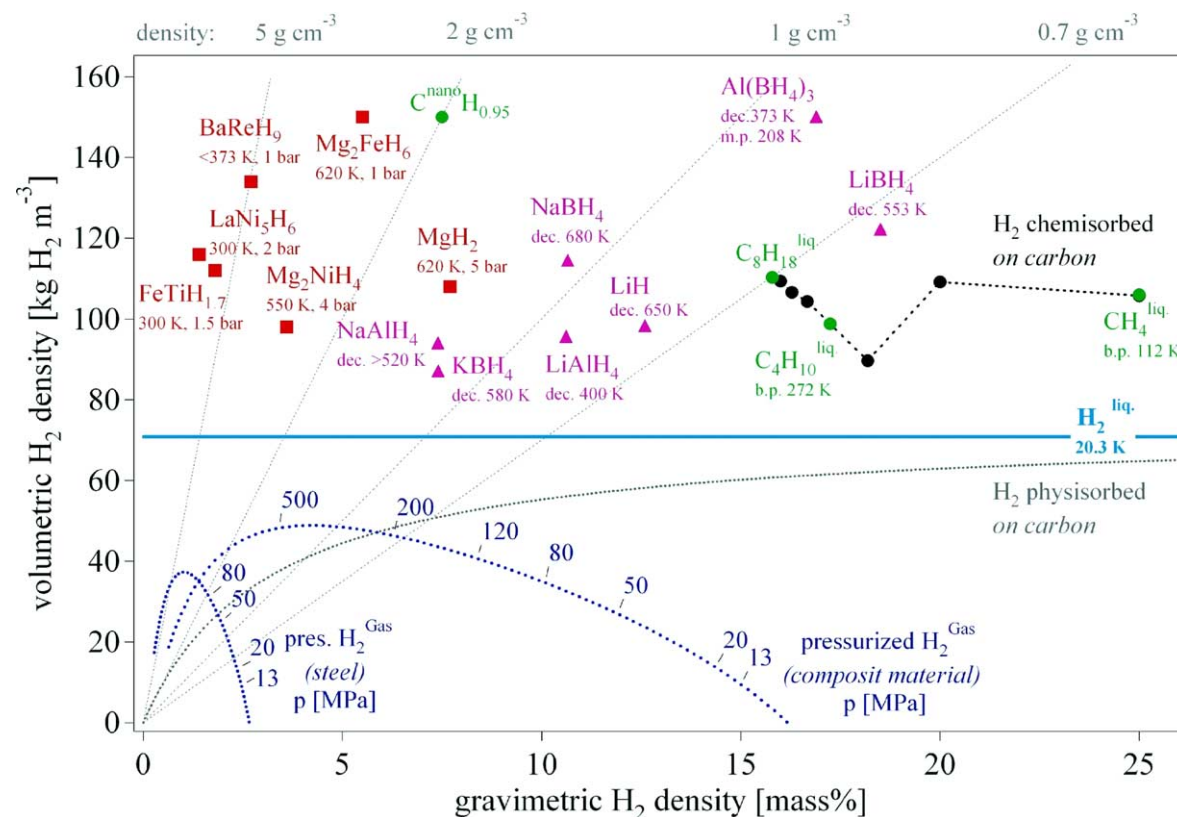


Fig. 6. Volumetric and gravimetric hydrogen density of some selected hydrides. Mg_2FeH_6 shows the highest known volumetric hydrogen density of 150 kg m^{-3} , which is more than the double of liquid hydrogen. $BaReH_9$ has the largest H/M ratio of 4.5, i.e. 4.5 hydrogen atoms per metal atom. $LiBH_4$ exhibits the highest gravimetric hydrogen density of 18 mass%. Pressurized gas storage is shown for steel (tensile strength $\sigma_v = 460 \text{ MPa}$, density 6500 kg m^{-3}) and a hypothetical composite material ($\sigma_v = 1500 \text{ MPa}$, density 3000 kg m^{-3}).

nanostructured palladium shows a narrowed miscibility gap (shorter plateau) and a reduced reversible hydrogen capacity. Physisorption of hydrogen on carbon converges to the density of liquid hydrogen, however, hydrogen adsorbed on high surface area carbons and nanotubes exhibits a low gravimetric density of less than 2 mass% and therefore also a low volumetric density. Zeolites and nanocubes behave like high surface area materials. No evidence for a new sorption phenomena apart from physis- and chemisorption was found. The complex hydrides exhibit very high volumetric and gravimetric hydrogen capacities. Due to the localization of the hydrogen atoms in the lattice these materials have to be investigated in there nano structured form.

Acknowledgements

This work was supported by the Swiss federal office of energy (Bundesamt für Energie, BfE) in contract with the International Energy Agency (IEA), the Swiss Federal Office of Education and Science (BBW), the European Commission (Fuchsia) and the Science Faculty of the University of Fribourg in Switzerland.

References

- [1] J.E. Lennard-Jones, *Trans. Faraday Soc.* 28 (1932) 333.
- [2] F. London, *Z. Physik* 63 (1930) 245;
F. London, *Z. Physik Chem.* 11 (1930) 222.
- [3] S. Brunauer, P.H. Emmett, *J. Am. chem. Soc.* 57 (1935) 1754;
S. Brunauer, P.H. Emmett, E. Teller, *J. Am. Chem. Soc.* 60 (1938) 309.
- [4] Y. Fukai, *Z. Phys. Chem.* 164 (1989) 165.
- [5] A.C. Switendick, *Z. Phys. Chem. N.F.* 117 (1979) 89.
- [6] D.J. Westlake, *J. Less-Common Met.* 91 (1983) 275–292.
- [7] A. Almendingen, G. Gundersen, A. Haaland, *Acta Chem. Scandina* 22 (1968) 328–334.
- [8] Ph. Buffat, J.-P. Borel, *Phys. Rev. A* 13 (6) (1976) 2287–2298.
- [9] Y. Jinlong, F. Toigo, W. Keli, *Surf. Rev. Lett.* 3 (1) (1996) 323–328.
- [10] A. Pundt, C. Sachs, M. Winter, T.M. Reetz, D. Fritsch, R. Kirchheim, *J. Alloys Compounds* 293–295 (1–2) (1999) 480–483.
- [11] G. Schmid, *J. Molec. Catal. A: Chem.* 107 (1996) 95.
- [12] A. Züttel, Ch. Nützenadel, G. Schmid, Ch. Emmenegger, P. Sudan, L. Schlapbach, *Appl. Surf. Sci.* 162–163 (2000) 571–575.
- [13] J. Farges, M.F. de Feraudy, B. Raoult, G. Torchet, *J. Chem. Phys.* 78 (1983) 5067.
- [14] J.W. Lee, G.D. Stein, *J. Chem. Phys.* 91 (1987) 2450.
- [15] E. Wicke, H. Brodowsky, in: G. Alefeld, J. Völkl (Eds.), *Hydrogen in Metals II*, Springer-Verlag, 1978, Chapter 3, p. 81.
- [16] A.C. Dillon, K.M. Jones, T.A. Bekkedahl, C.H. Kiang, D.S. Bethune, M.J. Heben, *Nature* 386 (1997) 377.
- [17] A.C. Dillon, et al., in: *Proceedings of the 2000 DOE/NREL Hydrogen Program Review*, 8–10 May 2000.
- [18] M. Hirscher, M. Becher, M. Haluska, U. Dettlaff-Weglikowska, A. Quintel, G.S. Duesberg, Y.M. Choi, P. Downes, M. Hulman, S. Roth, I. Stepanek, P. Bernier, *Appl. Phys. A* 72 (2001) 129.
- [19] S.J. Gregg, K.S.W. Sing, *Adsorption, Surface Area and Porosity*, Academic Press, London, New York, 1967.
- [20] G. Stan, M.W. Cole, *Low Temp. Phys.* 100 (1998) 539.
- [21] M. Rzepka, P. Lamp, M.A. de la Casa-Lillo, *J. Phys. Chem. B* 102 (1998) 10849.

- [22] K.A. Williams, P.C. Eklund, *Chem. Phys. Lett.* 320 (2000) 352.
- [23] S.M. Lee, K.H. An, Y.H. Lee, G. Seifert, T. Frauenheim, *J. Korean Phys. Soc.* 38 (2001) 686;
S.M. Lee, Y.H. Lee, *Appl. Phys. Lett.* 76 (2000) 2879.
- [24] Y. Ma, Y. Xia, M. Zhao, R. Wang, L. Mei, *Phys. Rev. B* 63 (2001) 115422.
- [25] W.B. Leung, N.H. March, H. Motz, *Phys. Lett.* 56 (1976) 425.
- [26] R.A. Beebe, J. Biscoe, W.R. Smith, C.B. Wendell, *J. Am. Chem. Soc.* 69 (1947) 95.
- [27] A. Züttel, P. Sudan, Ph. Mauron, T. Kyiobaiashi, Ch. Emmenegger, L. Schlapbach, *Int. J. Hydrogen Energy* 27 (2002) 203.
- [28] Y. Ye, C.C. Ahn, C. Witham, B. Fultz, J. Liu, A.G. Rinzier, D. Colbert, K.A. Smith, R.E. Smalley, *Appl. Phys. Lett.* 74 (1999) 2307.
- [29] C. Liu, Y.Y. Fan, M. Liu, H.T. Cong, H.M. Cheng, M.S. Dresselhaus, *Science* 286 (1999) 1127.
- [30] Y.Y. Fan, B. Liao, M. Liu, Y.L. Wei, M.Q. Lu, H.M. Cheng, *Carbon* 37 (1999) 1649.
- [31] P. Chen, X. Wu, J. Lin, K.L. Tan, *Science* 285 (1999) 91.
- [32] M. Hirscher, M. Becher, M. Haluska, A. Quintel, V. Skakalova, Y.M. Choi, U. Dettlaff-Weglikowska, S. Roth, I. Stepanek, P. Bernier, A. Leonhardt, J. Fink, *J. Alloys Compounds* 330–332 (2002) 654.
- [33] R. Ströbel, L. Jörissen, T. Schliermann, V. Trapp, W. Schütz, K. Böhmhammel, G. Wolf, J. Garche, *J. Power Sources* 84 (1999) 221.
- [34] M.G. Nijkamp, J.E.M.J. Raaymakers, A.J. van Dillen, K.P. de Jong, *Appl. Phys. A* 72 (2001) 619.
- [35] Ch. Nützenadel, A. Züttel, L. Schlapbach, *Electronic properties of novel materials, science and technology of molecular nanostructures*, in: H. Kuzmany, J. Fink, M. Mehring, S. Roth (Eds.), *American Institute of Physics, New York*, 1999, Chapter 9, p. 462.
- [36] Ch. Nützenadel, A. Züttel, Ch. Emmenegger, P. Sudan, L. Schlapbach, *Sciences and applications of nanotubes*, in: M.F. Thorpe (Ed.), *Fundamental Materials Research Series*, Kluwer Academic Publishing/Plenum Press, Chapter 10, p. 205.
- [37] A. Züttel, P. Sudan, Ph. Mauron, Ch. Emmenegger, T. Kiyobayashi, L. Schlapbach, *J. Metastable Nanocryst. Mater.* 11 (2001) 95.
- [38] S.M. Lee, K.S. Park, Y.C. Choi, Y.S. Park, J.M. Bok, D.J. Bae, K.S. Nahm, Y.G. Choi, S.Ch. Yu, N. Kim, T. Frauenheim, Y.H. Lee, *Synth. Met.* 113 (2000) 209.
- [39] J. Weitkamp, M. Fritz, S. Ernst, *Int. J. Hydrogen Energy* 20 (12) (1995) 967–970.
- [40] H.W. Langmi, A. Walton, M.M. Al-Mamouri, S.R. Johnson, D. Book, J.D. Speight, P.P. Edwards, I. Gameson, P.A. Anderson, I.R. Harris, *J. Alloys Compounds* 356–357 (2003) 710–715.
- [41] N.L. Rosi, J. Eckert, M. Eddaoudi, D.T. Vodak, J. Kim, M. O’Keeffe, O.M. Yaghi, *Science* 300 (2003) 1127–1129.
- [42] B. Bogdanovic, M. Schwickardi, *J. Alloys Comp.* 253–254 (1997) 1–9.
- [43] B. Bogdanovic, R.A. Brand, A. Marjanovic, M. Schwickardi, J. Tolle, *J. Alloys Compounds* 302 (1–2) (2000) 36–58.
- [44] T.N. Dymova, N.G. Eliseeva, S.I. Bakum, Y.M. Dergachev, *Dok. Akad. Nauk USSR* 215 (1974) 1369.
- [45] H.J. Schlesinger, H.C. Brown, *J. Am. Chem. Soc.* 62 (1940) 3429–3435.
- [46] H.J. Schlesinger, H.C. Brown, H.R. Hoekstra, L.R. Rapp, *J. Am. Chem. Soc.* 75 (1953) 199–204.
- [47] D. Goerrig, *German Patent* 1,077,644 (1958).
- [48] G.N. Schrauzer, *Naturwissenschaften* 42 (1955) 438.
- [49] S.J. Lippard, D.A. Ucko, *Inorg. Chem.* 7 (1968) 1051.
- [50] W.N. Lipscomb, *Boron Hydrides*, Benjamin, New York, 1963.
- [51] A. Züttel, P. Wenger, S. Rensch, P. Sudan, Ph. Mauron, C. Emmenegger, *J. Power Sources* 5194 (2003) 1–7.
- [52] P. Sudan, P. Wenger, Ph. Mauron, A. Züttel, *Letter to Nature Materials*, 2003, submitted for publication.
- [53] M. Fichtner, O. Fuhr, O. Kircher, J. Rothe, *Nanotechnology* 14 (2003) 778–785.
- [54] J.A. Northby, *J. Chem.* (1987) 6166.